Materials & Design 235 (2023) 112418

Contents lists available at ScienceDirect

Materials & Design

journal homepage: www.elsevier.com/locate/matdes

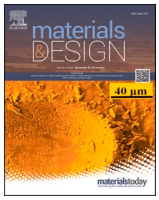

Development of open-pore polymer and ceramic foams/Guefoams with tunable fluid-dynamic properties: Application in highly efficient water bacteria removal

M. Guidoum [a], N. Verdú [a], J.L. Todolí [b], L.P. Maiorano [a], J.M. Molina [a,c,*]

[a] University Materials Institute of Alicante, University of Alicante, Ap. 99, E-03690 Alicante, Spain
[b] Analytical Chemistry, Nutrition & Food Sciences Department, University of Alicante, Ap. 99, E-03080 Alicante, Spain
[c] Inorganic Chemistry Department, University of Alicante, Ap. 99, E-03690 Alicante, Spain

ARTICLE INFO

Keywords:
Guefoam
Ceramic matrix
Polymer matrix
Activated carbon
Filtration
Bacteria

ABSTRACT

The usual replication method for preparing open-pore metal foams using NaCl as a template cannot be successfully applied to the fabrication of foams using either water-based ceramic slurries in which NaCl can be dissolved during processing, or liquid polymers that wet NaCl and leave no interconnecting windows between pores. In this work, we propose to modify the replication process by including a second template, paraffin, which is deposited over the NaCl and serves a dual purpose: (i) it acts as a barrier to dissolution of the NaCl with the matrix precursor, and (ii) it creates size-controllable binding collars between the particles that ensure the formation of interconnecting windows in the foam. The usefulness of the process described here is illustrated by the fabrication of two types of materials: low porosity epoxy and cement matrix foams and Guefoams. As proof of concept, epoxy-based Guefoams were developed for the removal of Escherichia coli in water using iodine-impregnated activated carbon particles as the guest phase. The results indicate that the Guefoams outperform conventional bactericidal particle beds in several aspects, including their ease of handling and their tunable fluid-dynamic properties that enable high bacteria annihilation efficiency.

1. Introduction

The use of open-pore foam materials is currently witnessing a rapid upswing in many technical applications. Since they are fluid-permeable materials, their uses encompass numerous applications including filtration, medical implantology, catalysis, pollutant retention, heat dissipation and energy absorption [1–3]. In recent years, the emergence of Guefoams, a novel foam material family, has sparked substantial interest owing to their multifunctionality, broadening the horizons of traditional foam applications. Guefoams incorporate functional phases (guest phases) within their cavities, sans chemical bonding, exhibiting notable efficiency in catalysis [4] and volatile organic compound (VOC) management [5,6]. Typically, open-pore foams and Guefoams are prepared using the versatile replication method, offering exceptional flexibility in material design. This method involves infiltrating a porous template preform with a liquid precursor, subsequently removing it through dissolution or chemical reaction. Notably, this approach surpasses other conventional manufacturing processes, primarily due to its ability to fine-tune pore geometry, size, and size distribution. The execution of this process varies according to the matrix type. In the case of metallic matrices, thermally resistant ceramic templates are often employed. Sodium chloride (NaCl), with a low melting point of 801 °C, serves as a popular template for low-melting metal precursors, such as aluminum, magnesium, and their alloys, due to its cost-effectiveness and abundance [7,8]. It can be processed into particles, typically spheres, by manually forming a paste of NaCl mixed with a binder like flour and water as a wetting agent [8–11]. The application of NaCl as a leachable template in ceramic and polymer foam preparation holds great appeal. However, its use for this purpose is constrained for two primary reasons: (i) the high solubility of NaCl in water leads to the partial or complete dissolution of the preform during infiltration with water-based ceramic slurries, and (ii) the strong wetting capacity of many polymers on NaCl results in complete pore space filling when infiltrated into NaCl-packed preforms, rendering NaCl dissolution and foam preparation unfeasible.

The scarcity of prior investigations into replication-based production of polymeric foams, particularly those utilizing template agents like

* Corresponding author at: University Materials Institute of Alicante, University of Alicante, Ap. 99, E-03690 Alicante, Spain.
E-mail address: jmmj@ua.es (J.M. Molina).

https://doi.org/10.1016/j.matdes.2023.112418
Received 4 May 2023; Received in revised form 13 October 2023; Accepted 18 October 2023
Available online 20 October 2023

sugar or salt (with emphasis on sodium chloride and calcium carbonate), has resulted in limited control over pore characteristics [12–14]. Among manufacturing techniques for polymer foams, direct foaming processes and additive manufacturing are the most common [15–17]. Ceramic foams, conventionally produced through various methods, including partial sintering, direct foaming, replica template, and sacrificial template [18–20], have relied extensively on the replica template technique. This involves impregnating an open-pore polymer foam with a ceramic suspension or precursor, yielding highly porous scaffolds with spherical pores [21]. The ability to adjust polymer foam properties allows for customizable pore sizes [22]. In contrast, the use of NaCl particles as a sacrificial template with aqueous-based liquid precursors lacks empirical support. Few prior studies have explored ceramic foam production via infiltrating packed NaCl particles with pre-ceramic polymers, such as policarboxilane to produce SiC foams [23] or synthetic mesophase pitch to manufacture graphite foams [24] and carbon matrix Guefoams [6]. These traditional methods are time-consuming and costly due to processing complexity and expensive starting materials.

In this study, the authors present an innovative modification of the replication method for fabricating polymer and ceramic matrix foams and Guefoams. This novel approach utilizes two templates, the first being NaCl in particulate form (for foams) or as a coating on a specific guest phase (for Guefoams), which is subsequently coated with paraffin (the second template) and sintered at low temperatures. The sintering process forms binding collars of controllable size between particles, creating interconnecting pores in the final materials. These paraffin-bonded preforms are then infiltrated with ceramic slurries or low-solubility polymers in paraffin. Once the matrix is consolidated, both templates can be easily removed. This innovative method empowers the production of open-pore foams and Guefoams, whether polymeric or ceramic in nature, offering an exceptional degree of design flexibility. It provides meticulous control over all factors influencing their ultimate fluid-dynamic attributes, encompassing pore geometry, dimensions, size distribution, and the structural attributes of the guest phases. This pioneering processing approach carries profound significance in the domain of customizing foam and Guefoam materials for precise applications. It signifies a notable breakthrough in extending the use of non-metallic materials into areas traditionally dominated by metallic foams, addressing the challenges associated with manufacturing foams of alternative compositions. As a proof of concept, epoxy-based Guefoams were developed and assessed for Escherichia coli removal using iodine-impregnated activated carbon particles as guest phases. The results demonstrate their potential as efficient water bacteria removal systems, surpassing conventional particle beds. The dual template replication process introduced here enables: (i) the fabrication of permeable monolithic foam structures that can be handled for regeneration and/or replacement in disinfection systems, and (ii) the generation of interconnecting windows with adjustable dimensions to achieve the attainment of desired filtration efficiencies.

2. Experimental procedures

2.1. Materials

The starting materials are sodium chloride (NaCl) particles with an angular geometry and a diameter within the range 20–38 μm (Panreac AppliChem GmbH, Germany), Nuchar RGC-30 activated carbon (AC) particles with a diameter in the range 1.2–2.4 mm (Westvaco - Chemical Division, USA) and solid paraffin (Merck KGaA, Germany). Images of these materials are shown in Fig. 1. Conventional cement supplied in sealed tubes (Sika, Spain) and Resoltech 1080S/1084 epoxy resin (CASTROComposites, Spain) were used as matrix precursors. High purity iodine (>99.8 %) and potassium iodide (>99.8 %) were used to functionalize the AC particles (Merck KGaA, Germany).

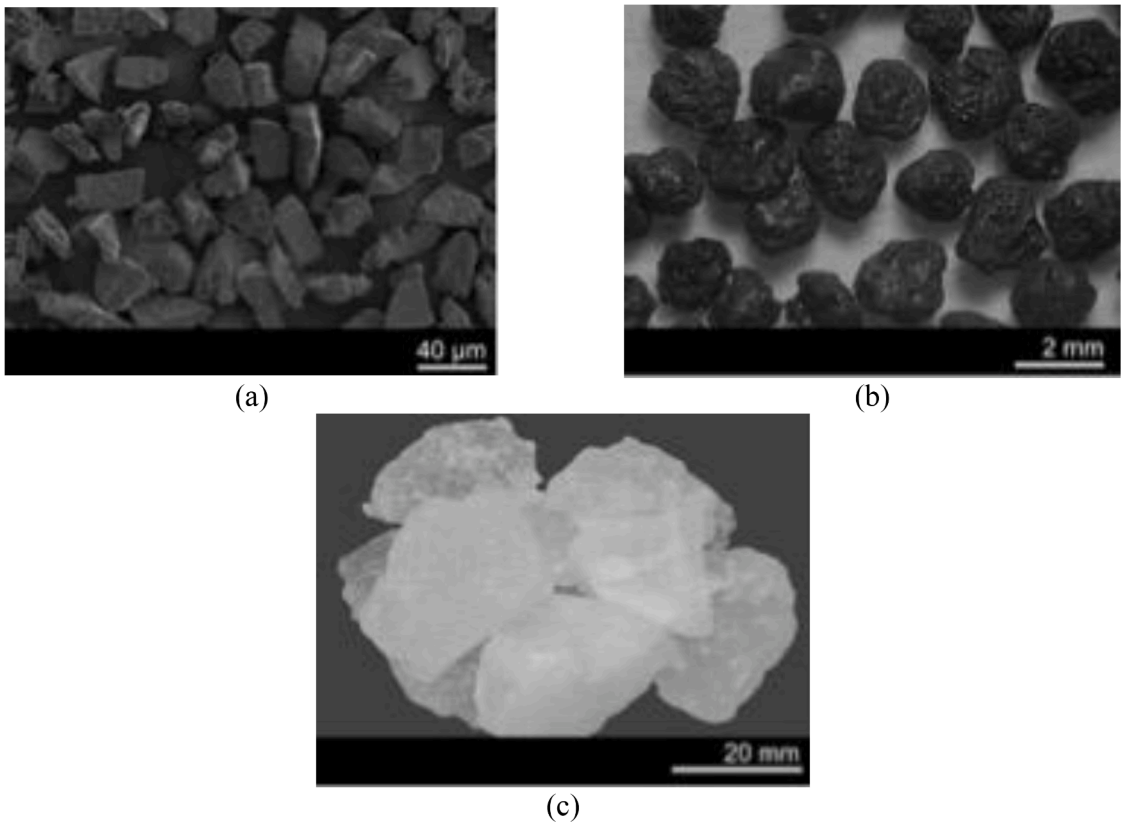

Fig. 1. SEM image of NaCl particles (a), and photographs of activated carbon particles (b) and paraffin blocks (c).

2.2. Preparation of NaCl spheres and NaCl-coated activated carbon (NaCl-AC) spheres

Following the procedure described in [10,25], NaCl particles were shaped into spheres of 1.8–2.5 mm in diameter. For this purpose, a mixture of commercial flour, sodium chloride and water in a ratio of 1:3:1 was prepared and hand-molded into small spherical particles. After drying at room temperature, these spheres were subjected to a two-step treatment: (i) carbonization of the organic binder at 200 °C for 60 min, and (ii) oxidation in air atmosphere at 500 °C for 6 h to remove much of the residual carbon. Even though the spheres may contain some residual binder, we refer to them as NaCl spheres for simplicity.

For the preparation of NaCl-coated activated carbon (NaCl-AC) spheres, the method described in [4–6] was followed. The AC particles were placed on an oscillating flat surface so that they could maintain some degree of rotational motion. They were then intermittently sprayed with a 20 % NaCl solution every 15 s. The total spraying time is proportional to the thickness of the NaCl coating.

2.3. Coating of the NaCl and NaCl-AC spheres with paraffin

The prepared spheres were coated with paraffin. For this purpose, about 30 g of paraffin were melted in a beaker heated to 60 °C. The spheres were then submerged into the liquid paraffin for 10 s. After being pulled out from the liquid paraffin, the spheres were placed on laboratory paper covering a tilting plate. The movement of the plate enables the paraffin to solidify homogenously and without dripping around the entire geometry of the spheres, maintaining a relatively uniform coating thickness.

2.4. Preparation of the preforms, infiltration and removal of the double template

The paraffin-coated sodium chloride spheres (either with or without AC at the core) were manually packed into a cylindrical borosilicate glass crucible with a diameter of 20 mm and a height of 150 mm. This procedure must be executed carefully to prevent spheres from fracturing. Packed in this way, the particles attained an approximate volume fraction of 0.58. This value is dependent on several variables, including the handling capacity of the operator, the dimensions of the crucible, and the shape, size and size distribution of the spheres. The crucible containing the preform was placed in a furnace at a temperature below the melting point (38 °C and 42 °C were tested in this study) for 0–50 min. The spheres that make up the preform were sintered by the partial melting and solidification of the paraffin that coats the spheres. It is normal for some paraffin to settle to the bottom of the crucible during this process, so that the lowest 5 mm of the preform were discarded. This operation results in the formation of paraffin binding collars between the spheres and, after the templates are removed, forms the interconnecting windows between the cavities of the material.

The crucible with the preform was then placed in a vacuum-capable glass infiltration chamber. First, the chamber was vacuumed to a pressure of 1 mbar, followed by the infiltration of the preform with the liquid precursor. Once enough liquid precursor had been transferred, the vacuum was released, and the chamber was pressurized to ensure complete filling of the porous preform with the liquid precursor. The type of precursor affects the infiltration pressures. In all cases of the present study, an infiltration pressure of 2 bar was used, which ensures complete filling of the pore space. After infiltration of the packed preforms with liquid cement precursor or epoxy resin, sufficient time (36 h and 24 h, respectively) was allowed for matrix consolidation, followed by the removal of excess matrix by standard machining procedures.

In the next step, both the NaCl and paraffin templates were removed. To do this, the sample was immersed in an ultrasonic distilled water bath (alternatively, for comparison, a magnetically stirred bath was utilized) at a temperature of 50 °C. The sample was then dried overnight at 30 °C. The procedure proposed in this work is shown schematically in Fig. 2.

For the removal of the double template, a special device was utilized to ensure total submersion of the samples in water since they lose density and tend to float as the removal process progresses. This device, depicted in Fig. 3, basically consists of a 20-mesh metal basket that keeps samples submerged. In addition to this function, the device prevents the molten paraffin released from interacting with the material by allowing it to remain in the water as supernatant liquid.

2.5. Preparation of epoxy Guefoams for water bacteria removal

To confer bactericidal properties to the prepared materials, the surface of the guest phase particles (activated carbon) was impregnated with molecular iodine, following a procedure slightly modified from the one proposed by Natori [26]. 1 g of I_2 and 1.5 g of KI were dissolved in 5 ml of distilled water and magnetically stirred in a flat-bottomed glass flask for 1 h at 250 rpm. 3 g of AC particles were added to the solution, which was then stirred for 24 h. The particles were then extracted from the solution and washed with 100 ml of distilled water using a Büchner funnel. The treated particles served two purposes: (i) the preparation of epoxy matrix Guefoams and (ii) the preparation of packed beds. Both Guefoams and particle beds were used in the antibacterial activity tests. Prior to use, the iodine coating elution was studied by injecting different amounts of distilled water through the materials at a pressure of 2 bar. For that purpose, Guefoams were encased in a PVC pipe connected to a pressurized water circuit. Teflon tape was used to provide a seal between the sample and the tube. The AC particles were packed as a bed in an analog PVC tube with two high permeability plugs screwed into the tube to maintain the position of the particle bed. The tube was connected to the water pressure circuit via these plugs.

2.6. Materials characterization

Morphological characterization of the AC and the prepared spheres was performed using scanning electron microscopy (SEM-Hitachi S3000N) and optical microscopy (Olympus PME3-ADL). In addition, image analysis software (Buehler-Omnimet Enterprise, Illinois, USA) was used to determine the geometrical parameters of the particles, such as size distribution and aspect ratio (AR, defined as AR = major axis diameter/minor axis diameter, with AR = 1 for perfect spheres). Thermal stability of the paraffin was determined by thermogravimetry (TG-Metler Toledo) in the range 50–600 °C in air and nitrogen atmospheres at a heating rate of 6 °Cmin^{-1}. Paraffin removal conditions were evaluated using differential scanning calorimetry (DSC-Q250 TA Instruments) in the temperature range 20–100 °C in air or nitrogen atmosphere at a heating rate of 5 °Cmin^{-1}. The specific surface area and pore size distribution were determined using the physical gas adsorption technique (N_2 adsorption isotherms at −196 °C) and the BET (Brunnauer-Emmet-Teller) theory. The modification of the AC surface with iodine was analyzed quantitatively using high-resolution scanning electron microscopy (SEM-Jeol IT500HR/LA) with an energy dispersive spectroscopy (EDS) detector, and the distribution of iodine was determined by elemental mapping.

In addition, the relative pressure drop (ΔP/ΔL) between the ends of the samples was determined by water injection measurements at 25 °C and a setup first described in [27]. To determine the flow rate, the mass of water leaving the sample at a given pressure was measured using a balance with an accuracy of ± 0.001 g. Water permeability (k) was derived from the well-known Darcy's law:

$$k = \frac{\mu}{(\Delta P/\Delta L)} v \tag{1}$$

where v is the fluid surface velocity (ratio of the volumetric flow rate to the total cross-sectional area of the pipeline), ΔP is the absolute pressure drop, ΔL is the sample length and μ is the fluid dynamic viscosity

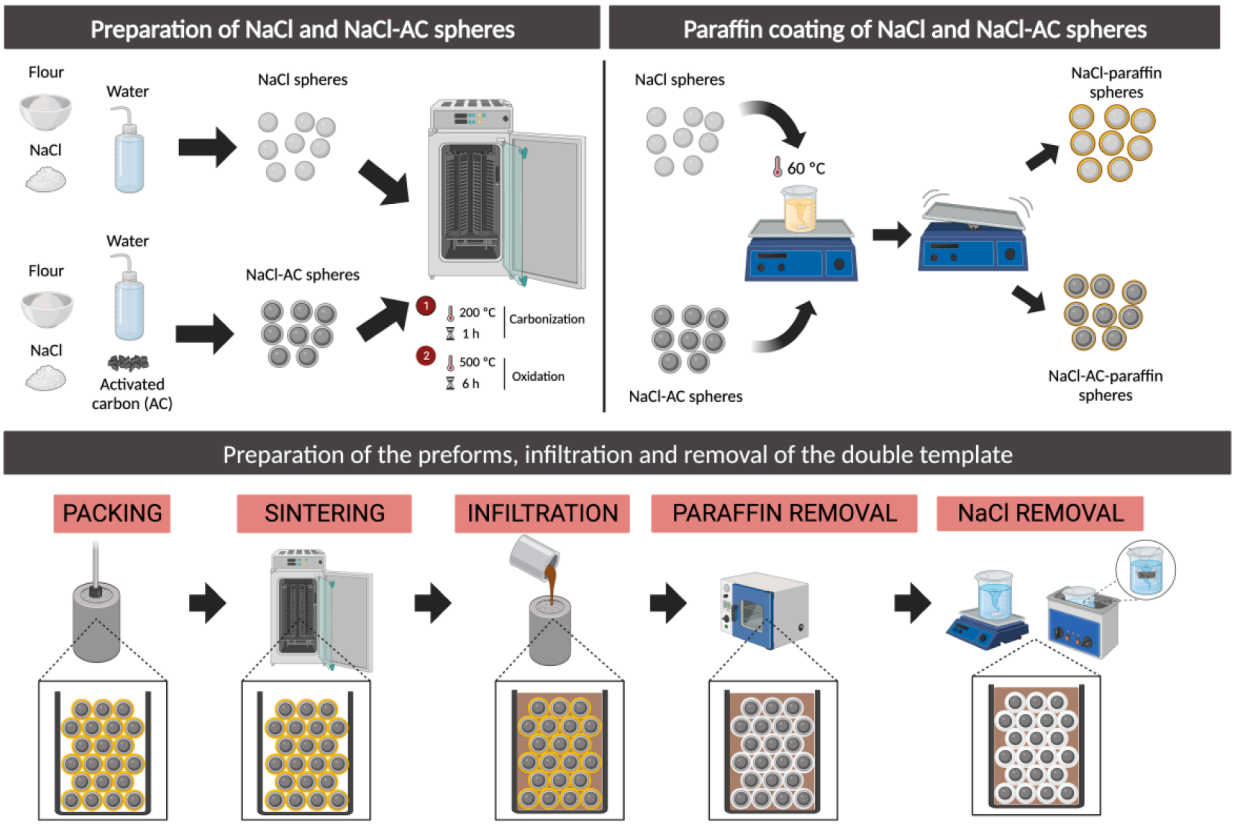

Fig. 2. Main steps in the preparation of foams and Guefoams.

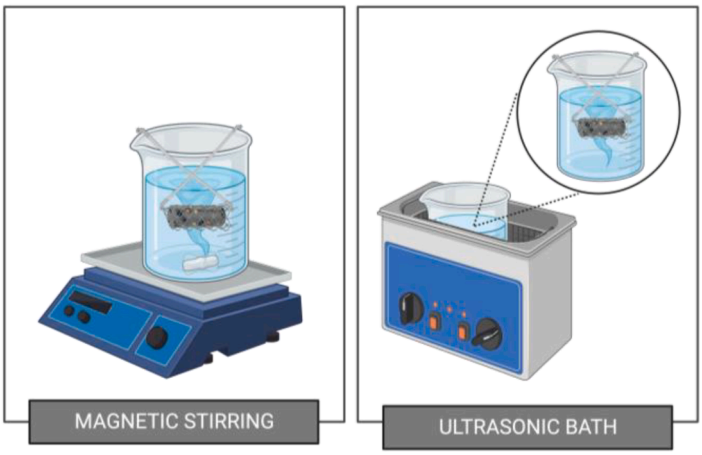

Fig. 3. Schematic of the devices used for the removal of the double template.

(assumed to be 1.003×10^{-3} $kgm^{-1}s^{-1}$ at 20 °C). The permeability error estimate was 8 %.

2.7. Antibacterial activity

Escherichia coli (*E. coli*) from the Spanish Type Culture Collection CECT 434 was selected as the bacterial strain for this study. First, *E. coli* were incubated in Tryptic Soy Broth (TBS) medium at 37 °C for 24–48 h and cultured until 0.5 McFarland standards (corresponding to 1.5×10^8 $CFUml^{-1}$) were reached. The bacteria suspension was diluted to about 10^2, 10^1 and 10^0 $CFUml^{-1}$ and kept for analysis. The antibacterial tests were performed using the device illustrated in Fig. 4. Teflon tape was used to seal the Guefoam samples to the funnel tube walls. For the 10^2 and 10^1 $CFUml^{-1}$ concentrations, a variable volume of diluted bacteria solution is passed through the materials to maintain a constant water flow rate. For that, the height (h) of solution above the samples must be maintained as the fluid flows through them. For a successful bacterial count, 1 ml of each filtrate was diluted 10–1000 times, from which 100 μl was spread on a Petri dish containing Rapid'E coli medium and incubated at 37 °C for 24 h. For the 10^0 $CFUml^{-1}$ concentration, employed in experiments devoted to test water purification for human consumption, a 5-liter volume was subjected to filtration using an optimized Guefoam material. The entire volume underwent processing through the standard membrane filtration method, and the bacteria remaining on the membrane were subsequently cultivated and incubated under the aforementioned conditions. Each test was conducted in

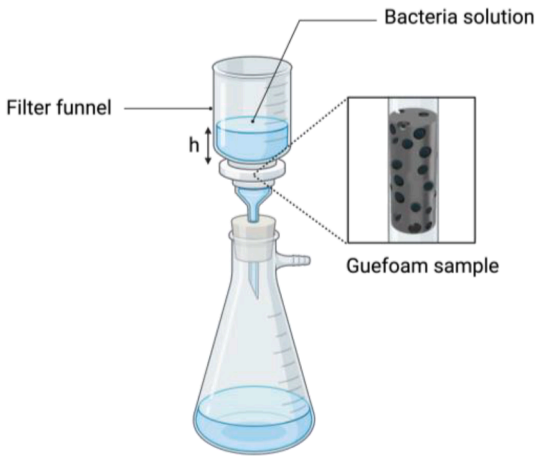

Fig. 4. Schematic of the filtration device used to remove bacteria from water.

quintuplicate.

3. Results and discussion

3.1. Microstructural characterization of NaCl spheres and NaCl-AC spheres

Fig. 5a-b display images of NaCl and NaCl-AC spheres, revealing that they were formed by the joining of smaller granular crystalline entities. Despite different processes were used to prepare the spherical particles of the NaCl and NaCl-AC systems (see Section 2.2), both types of particles exhibited similar morphologies characterized by a high degree of regularity (nearly spherical morphology) and a significant degree of porosity visible in the microscopic images of their surfaces (Fig. 5c-d). These regular morphologies are attributable to the versatility and successful optimization of the employed processes. On the one hand, the consistency of the flour-NaCl-water mixture was suitable for hand molding. On the other hand, the coating achieved by successive spraying with NaCl solution prevented the irregular morphology of the AC particles (Fig. 1b) from being transferred to the NaCl-AC particulate entities, so that they acquired regularity and sphericity as the coating thickness increased. Fig. 5d shows the NaCl coating thickness at which quasi-spherical geometries were achieved in the NaCl-AC system, corresponding to about 200 μm. Fig. 5e displays the particle size distributions for the systems AC, NaCl and NaCl-AC. AC particles had an average diameter of 1.80 mm while NaCl and NaCl-AC spheres had average diameters of about 2.20 and 2.30 mm, respectively. Fig. 5f shows values for aspect ratio of 1.22 for the AC particles, 1.12 for the NaCl system and 1.13 for the NaCl-AC system, the last two indicating high degree of sphericity.

3.2. Paraffin coating of the spheres and sintering of the preforms

Fig. 6a-d depict how the paraffin coating modified the surface morphology of the spheres. In general, the paraffin coating resulted in a compact and uniform surface with a smooth texture and no major defects (Fig. 6c-d). The micrographs in Fig. 6e-f illustrate the interparticle binding collars formed during sintering of the packed preforms. The size of these collars, which bound the spheres to form self-standing preforms, could be controlled by modifying the temperature or sintering time.

Fig. 7a shows the findings of a study in which the dimensions of the interparticle binding collars were investigated as a function of sintering time under two temperatures. With temperature, the sintering process was accelerated, and the growth became more time-consuming with increasing binding collar diameter, as would be expected from the classical sintering densification curves of particulate materials [28]. The evaluated conditions resulted in the formation of binding collars that allowed the creation of interconnecting window sizes in the range 0.2–0.8 mm, so that the derived foams would exhibit pressure drop values that could be adapted to a wide range of technological applications.

The kinetics of the sintering process leading to the formation of interparticle binding collars can be interpreted using the theoretical model proposed by Kuczynski [29], which was developed for the bonding of particles with spherical geometry:

$$\left(\frac{x}{a}\right)^n \approx Bt \tag{2}$$

where x/a is the ratio of collar and particle average radii, B is a parameter related to the temperature and certain geometrical and property parameters of the particles, t is the sintering time, and n is an exponent that allows defining the dominant mechanism during the process. Equation (2) could be represented as log × versus log t to obtain the parameter n (Fig. 7b). Linear least squares regressions of the data shown in Fig. 7b related the slope of the line to the reciprocal of n and yields a value for the two explored temperatures of n≈ 2. This value corresponded to a sintering mechanism in which a combination of viscous and plastic flow was dominant, as found in the analysis of [30].

3.3. Elimination of the double-template in preforms

Thermogravimetric analysis of the paraffin was performed to determine the optimum conditions for its complete removal. Fig. 8 depicts the TG/DTG and DSC thermograms of paraffin in nitrogen and air atmospheres. The TG and DTG curves under nitrogen showed the thermal stability of paraffin from room temperature to about 150 °C (Fig. 8a). In agreement with the temperatures reported by [31,32], the decomposition of paraffin, which represented the breakdown of hydrocarbons into hydrogen and carbon molecules, occurred in a single step between about 150 °C and 290 °C (some variations may be attributed to the purity of the material or the heating rate). When the analysis was performed in air, the TG curve shifted to lower temperatures (about 20 °C lower than in an inert atmosphere, as reported by [33]). The paraffin began to lose stability at about 130 °C, leading to complete mass loss at about 255 °C. The DSC curves under both atmospheres revealed two characteristic peaks: one in the 25–30 °C range, corresponding to a solid–solid phase transition with low heat flux, and another peak in the 35–50 °C range, corresponding to a solid–liquid phase transition with a higher associated heat flux (Fig. 8b) [31,34].

Based on these findings, it was decided to test the removal of both templating agents in a single step using water at 50 °C. It was assumed that water at this temperature facilitated both the dissolution of the NaCl and the melting of the paraffin, which floated on the water due to its low density. To aid in the removal of the double template, the tempered water was either magnetically stirred or sonicated. It was found that for both treatments the preforms were completely eliminated at times below 60 s for both NaCl and NaCl-AC spheres. Fig. 9 shows, as an example, a sequence of photos taken during the removal process in magnetically stirred 50 °C water of NaCl-AC spheres. The upper part of the beaker was fogged due to water evaporation at the working temperature. When the removal of the templating agents was complete, the water acquired certain opacity and the AC particles were released and tend to float over the water (in the photo of Fig. 9c, some AC particles were observed on the surface of the water and others were still in suspension).

These AC particles retained a high specific surface area of 975 m^2g^{-1}, albeit 25 % lower than that of the pristine AC particles (1295 m^2g^{-1}), most likely because a small amount of the templating agents was retained in the pores of the activated carbon. These residues were negligible in terms of mass but significantly affected the specific surface area value. However, no discernible micrographic differences (Fig. 10a-b) were observed on the surface of the activated carbon as a result of the

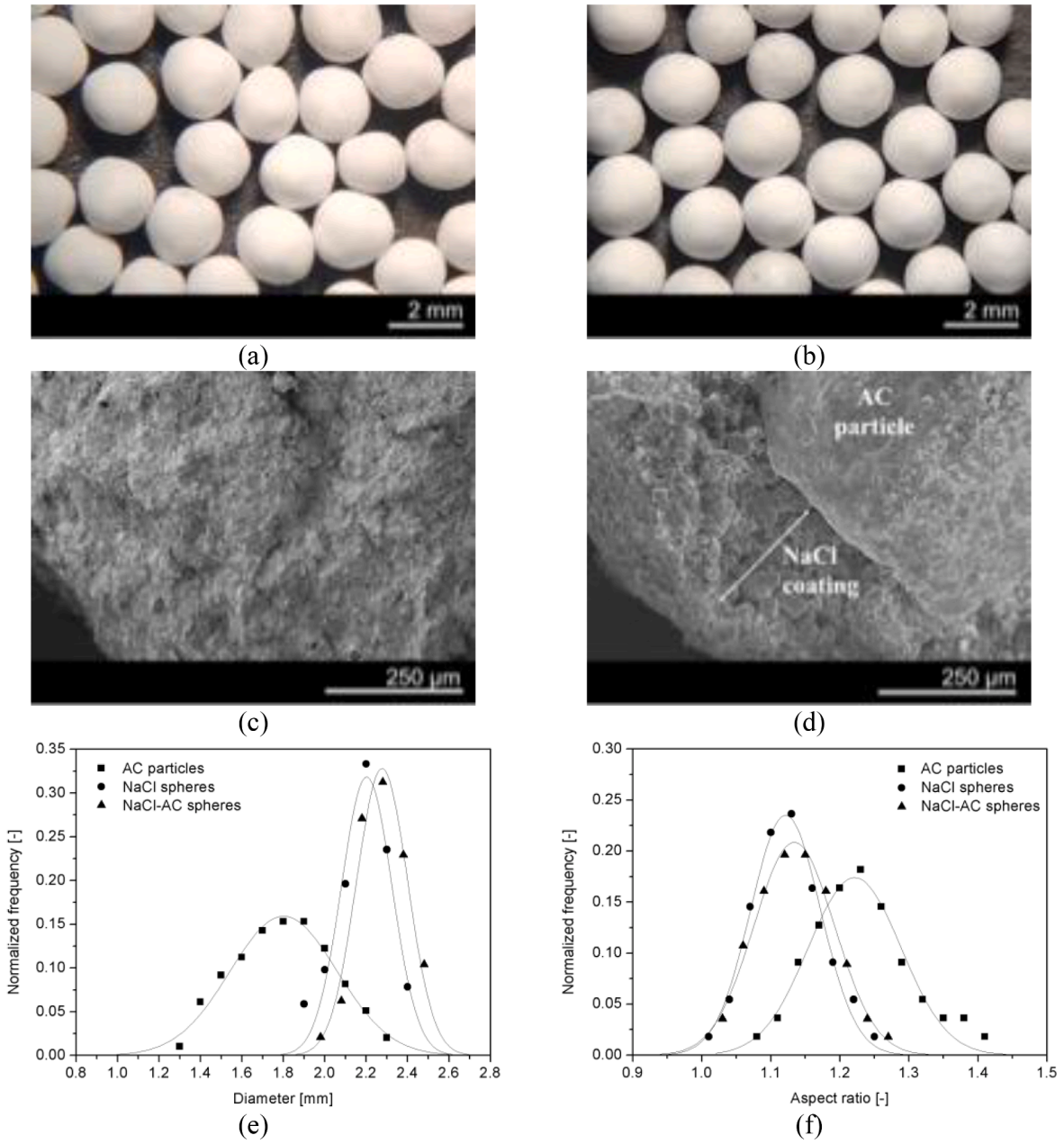

Fig. 5. Photographs (a,b) and SEM images (c,d) of: NaCl spheres prepared by the procedure described in [10,25] (a,c) and NaCl-AC spheres prepared by the procedure described in [4–6] (b,d); (e,f) are the distributions of the diameter and aspect ratio, respectively, of the AC and prepared spheres.

removal of the templating agents. The pore size distributions calculated from the desorption curves (Fig. 10c-d) indicated that the only affection of the removal process was in the sense of decreasing the number of fine pores in the activated carbon. In view of these results, in another experiment, a representative amount of AC particles was taken after the template agent removal treatment and subjected to ultrasound in hexane for 10 min. The specific surface area value (1250 m^2g^{-1}) (Fig. 10c-d) was consistent (only about 3.5 % less) with that of the pristine AC particles, indicating that the residue remaining in the finest pores of the activated carbon was most likely paraffin, since paraffin, and not NaCl, is highly soluble in this solvent.

3.4. *Examples of fabrication: Ceramic and polymer foams and Guefoams with AC particles as the guest phase*

As examples demonstrating the feasibility of the proposed processing route, the materials listed in Table 1 were produced. These materials included epoxy and cement matrix foams and Guefoams. For their fabrication, the previously described steps were followed and a paraffin sintering time of 30 min at 42 °C was used.

The dissolution of the double template was carried out by magnetic stirring and ultrasound for comparison. To avoid the undesired effect of paraffin contamination of the AC, the device illustrated in Fig. 3 was used. This device kept the sample submerged during the removal process and away from the molten supernatant paraffin, thus preventing the liquid paraffin from interacting with the sample and avoiding undesirable redeposition. Fig. 11 shows the results of both methods in terms of normalized mass loss as a function of time. The normalized mass loss is defined as follows:

$$m_n = 1 + \frac{m - m_o}{m_t} \tag{3}$$

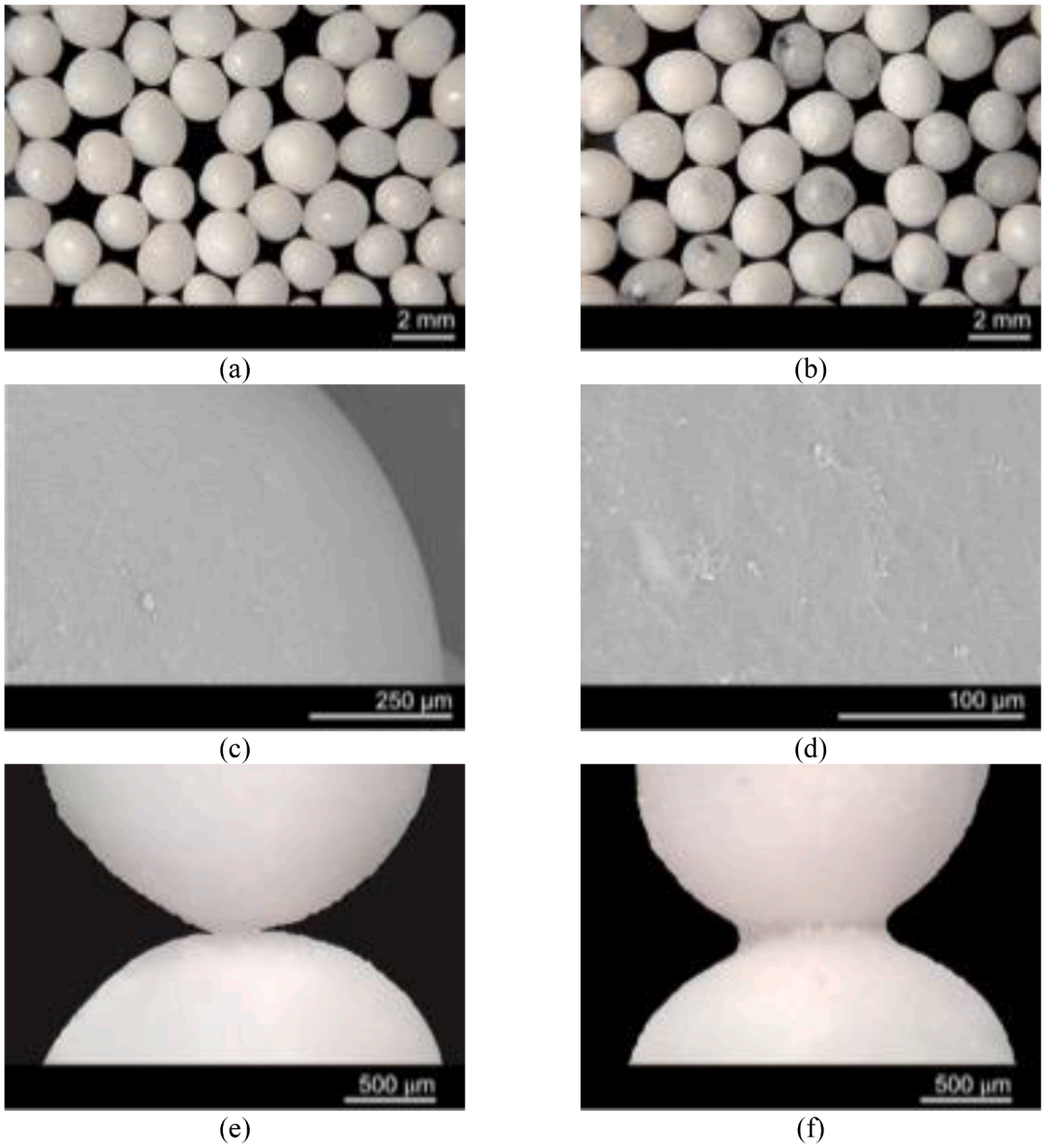

Fig. 6. Photographs of NaCl (a) and NaCl-AC (b) spheres, both coated with paraffin; high magnification SEM images showing the paraffin coating of a NaCl sphere (c, d); micrographs of the binding collars between two NaCl spheres formed by the sintering process for 5 (e) and 50 (f) min at 42 °C.

where m_o and m are the initial and instantaneous masses of the sample, respectively, while m_t is the total mass of the two templating agents (estimated experimentally from the difference in mass between the double-coated and uncoated particles). The removal efficiency of the templating agents was higher for ultrasonic treatment since complete removal was achieved in about 3 h for foams and 5 h for Guefoams. These times were ostensibly longer than those recorded for the removal of non-infiltrated preforms because, after infiltration, water must access the spheres comprising the preform through the interconnecting windows of the material. Recorded dissolving times, far from being universal for a particular dissolution procedure, therefore depended on the size of the interconnecting windows, with favorable dissolution being observed as window size increases. Additionally, the mass loss data for a material denoted as sample M, which was manufactured by infiltrating a preform made of packed uncoated NaCl spheres (lacking paraffin coating) with epoxy resin, is presented in Fig. 11. The results suggest that both dissolution methods resulted in a mass loss of less than 10 %, indicating that complete removal of the NaCl template agent was not achieved. Another material was fabricated using a similar preform, in this case infiltrated with the same water-based precursor suspension of cement ceramic matrix that was employed in the current study. The absence of paraffin resulted in partial dissolution of NaCl during infiltration, which ultimately led to structural collapse before achieving full matrix consolidation. Both experiments provided evidence for the significant role of paraffin as a secondary template agent.

An analysis of the specific area of the AC particles in these materials (extracted with extreme care from the outermost cavities of the material) revealed a value of 1235 m^2g^{-1}, which was only 4.5 % less than the value found for the pristine AC particles, demonstrating the efficacy of the device depicted in Fig. 3, which avoided the use of the environmentally unfriendly chemical hexane.

Fig. 12a-d show the dimensions and microstructures of the conventional foam samples developed from ceramic (cement) and polymer (epoxy resin) precursors. Fig. 12e-f show magnified images of Guefoams with both types of matrices and with AC particles as the guest phases in the porous cavities. Despite the lack of detailed scale-up research for this

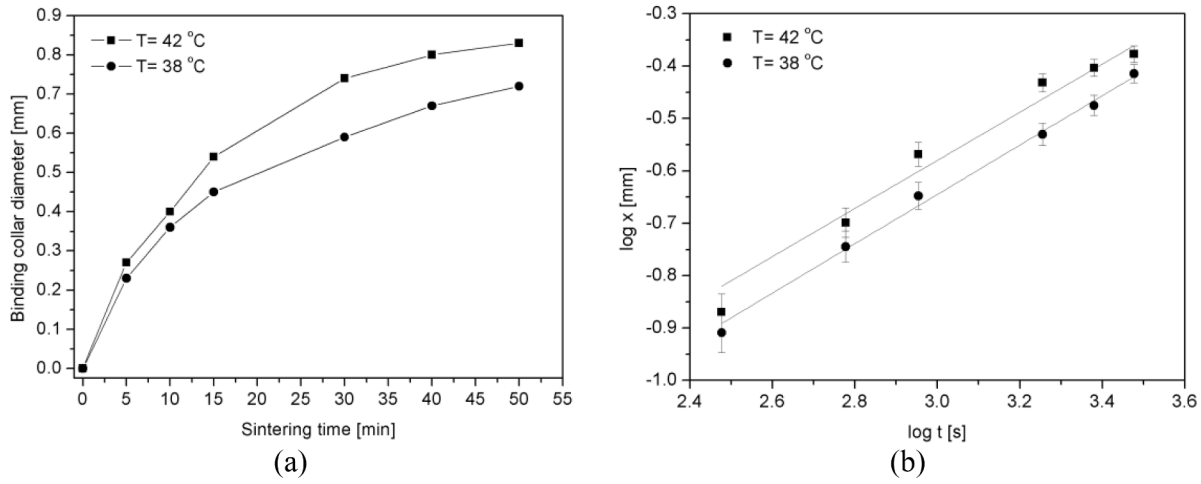

Fig. 7. Average diameter of interparticle binding collars as a function of sintering time at 38 and 42 °C (a); (b) is a double logarithmic representation of the data in (a). The linear fitting equations in (b) are: y = 0.49x-2.07 and R^2 = 0.98 for T = 42 °C; y = 0.48x-2.08 and R^2 = 0.99 for T = 38 °C.

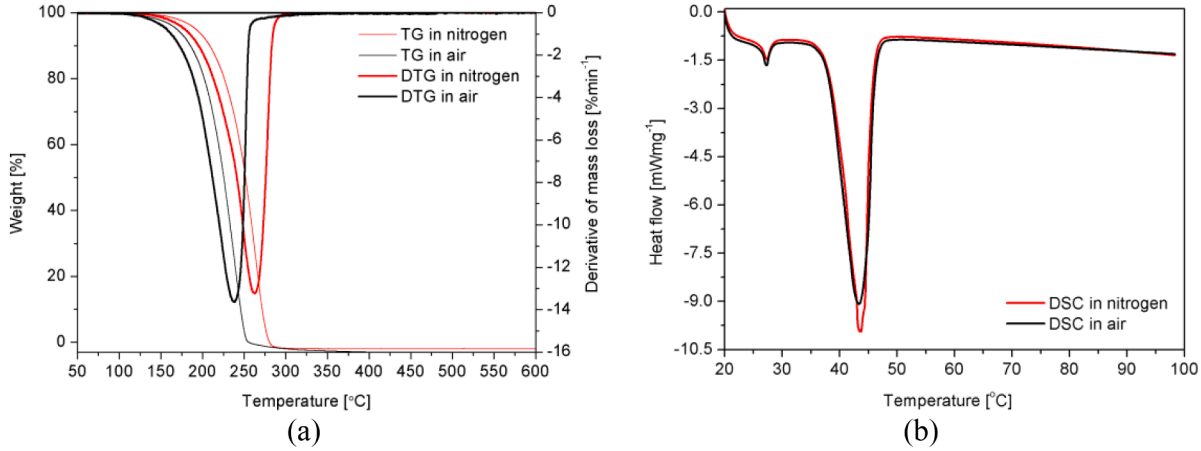

Fig. 8. TG/DTG (a) and DSC (b) curves of paraffin in nitrogen and air atmospheres.

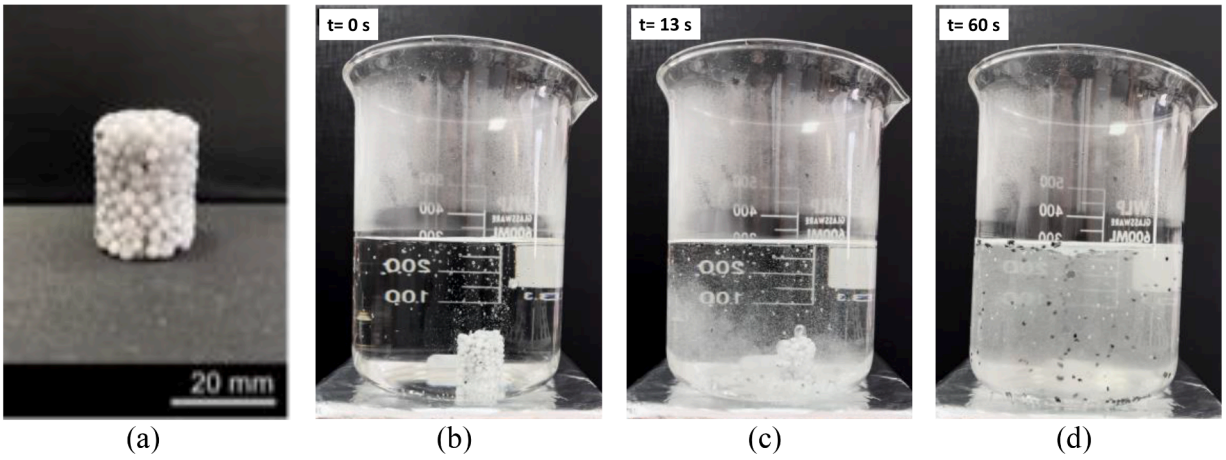

Fig. 9. Sequence of photos taken during the dissolution process of a preform prepared with NaCl-AC spheres in magnetically stirred water at 50 °C. The photo in (a) corresponds to a sintered preform before dissolution.

procedure, it is important to note that the dimensions of these samples were not constrained by any manufacturing step. In fact, samples up to three times larger in dimensions were produced and no obstacles to the production of high-quality products were found.

The structure of Guefoams is characterized by two main parameters, guest loading (GL) and guest occupation (GO), as defined in [4–6]:

$$GL = \frac{number\ \ of\ \ pores\ \ hosting\ \ a\ \ guest\ \ phase}{total\ \ number\ \ of\ \ pores} \quad (4)$$

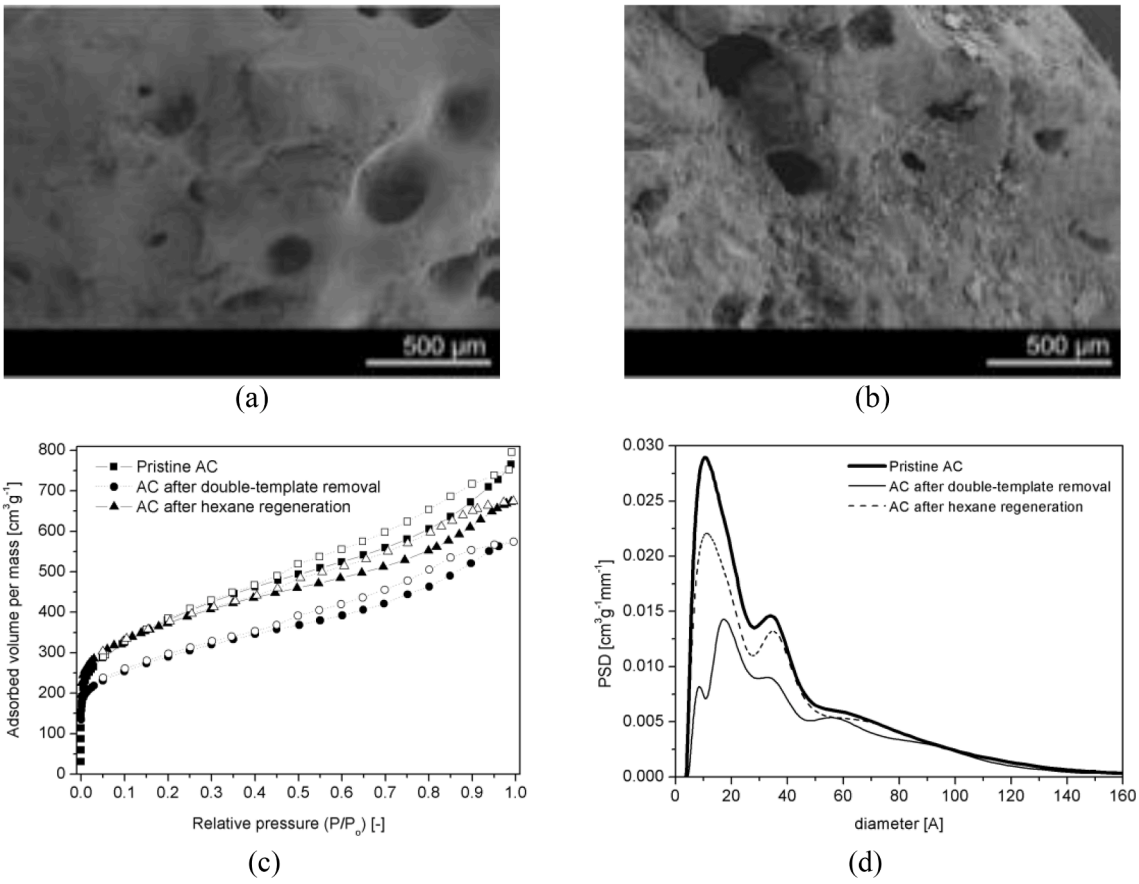

Fig. 10. SEM images of (a) AC particles in the initial state and (b) after removal of the double-template; nitrogen adsorption–desorption isotherms at −196 °C (c) and pore size distributions (d) of AC particles in three states: as received, after removal of the double template and after regeneration treatment with hexane.

Table 1
Fabricated materials and their main properties. GL and GO denote the guest loading and guest occupation, respectively, calculated using Equations (4–5); D is the average pore diameter and Vp refers to pore volume fraction.

Samples	Code	matrix	D (mm)	GL (%)	GO (%)	Vp
Foams	F-e	epoxy	2.20	–	–	0.59
	F-c	cement				0.57
Guefoams	G-e	epoxy	2.19	1.00	0.51	0.58
	G-c	cement				0.57

$$GO = \frac{volume\ \ of\ \ a\ \ guest\ \ phase}{volume\ \ of\ \ its\ \ hosting\ \ pore} \tag{5}$$

GL denotes the fraction of pores hosting a guest phase while GO denotes the average cavity volume fraction occupied by a guest phase. When about 200 NaCl-AC freshly prepared spheres were intentionally broken, each was found to contain a single AC particle; therefore, the GL parameter of the samples was estimated to be 1 (see Table 1). Since both the guest phase and the spheres produced by NaCl coating had a nearly spherical geometry, image analysis could be used to determine the GO parameter from their average diameter estimations. According to Equation (5), GO can be simply expressed as $GO = (d/D)^3$, where d is the average guest phase (AC particles) diameter and D is the average diameter of the NaCl-coated guest phase (corresponding to that of the hosting pores in the foam). GO is about 0.51 (Table 1). Regarding the pore volume fraction (Vp), the values for the foams were consistent with those published by Langston et al. [35], who reported a packing volume fraction of 0.57 for NaCl spheres packed in crucibles that had a 9:1 crucible-to-particle diameter ratio (as is the case in the present study).

To assess the microstructural quality of the newly developed materials, the number of interconnecting windows per pore (also referred to as coordination number) was counted in both foam types. The coordination number in Guefoams was determined after removing the guest phases of the outermost pores of the samples. The results are shown in Fig. 12g, which indicates that the coordination number in foams and Guefoams was comparable regardless of the type of matrix. The most frequent value was 7, which corresponded to those previously reported for metallic foams obtained using the replication method [36,37]. The fluid dynamic behavior of a porous material obtained by replication is determined by the coordination number, the pore size and the size of the interconnecting windows, the latter being the crucial parameter for the permeability of the foam [11,27,37–39]. By changing the size of the interconnecting windows, the pressure drop of a given material can be modified. Fig. 12h depicts the size distributions derived from a thorough image analysis of the fabricated materials. All samples had an average window size in the range 0.73–0.75 mm.

3.5. Suitability of polymer Guefoams for water bacteria removal

The antibacterial activity of the prepared materials (Table 2) was based on the iodination of the AC particles, which acted as the guest phases. For comparison, activated carbon (AC) and iodinated activated carbon (I-AC) packed beds were tested.

Considering their potential application for the removal of pathogenic microorganisms in water, it is critical to understand the stability of the iodine coating upon water washout. Fig. 13a shows a micrograph with a mapping of the element iodine on the surface of an AC particle extracted from a Guefoam sample (G-3 in Table 2). The percent mass of iodine was quantified using EDS for two samples, a densely packed bed of I-AC

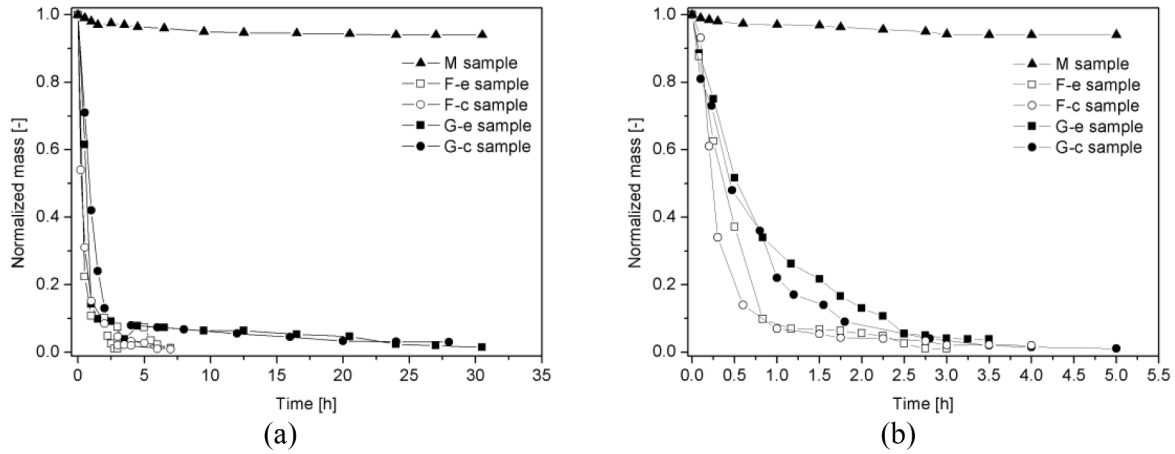

Fig. 11. Normalized mass loss during dissolution of the double template in water at 50 °C for foams and Guefoams under magnetic stirring (a) and ultrasound (b). The graphs also depict information regarding a sample M, which was fabricated by infiltrating a preform prepared by packing NaCl spheres without paraffin coating with epoxy resin.

particles and the sample G-3, through which controlled amounts of distilled water were injected. The results for I-AC particles are shown in Fig. 13b, where each point on the graph represents the average of five independent measurements. A nonlinear relationship was observed between iodine elution and the volume of water washout. There was an initial significant decrease of 11 % iodine after the flow of 50 l of water, followed by stabilization up to a total volume of 200 l. This behavior was consistent with that observed in the original studies of [26], in which the bactericidal activity of iodine-treated activated carbons was maintained up to 10^4 l of water (according to the results of [26], the water treatment capacity of iodine-coated activated carbons was about 7 lm^{-2}). Therefore, it could be stated that the stability of these coatings is commensurate with their applicability as water filters. A similar study conducted with the G-3 sample yielded comparable results. However, it should be noted that the fluid dynamic conditions created when water flows through particle beds and Guefoams may be different, which may affect the elution behavior after large volumes of water have passed through.

When evaluating materials manufactured to remove bacteria in water, it was necessary to determine the pressure drop experienced by the fluid as it passed through. To that end, the water pressure drop at various velocities was measured in the particle beds and Guefoams of Table 2, the latter being materials with varying interconnecting window sizes (Fig. 14a). At first glance, the relative pressure drop was dependent on the dimensions of the interconnecting windows, with the packed particle beds exhibiting a relative pressure drop intermediate between that of G-2 and G-3 materials. In Fig. 14b the data of Fig. 14a were recasted as reduced relative pressure drop, which was obtained by dividing ΔP/ΔL by v. The experimental results revealed that water exhibited linear behavior with nil slopes, indicating that the fluid dynamic regime was fully laminar or Darcian.

From the fitting equations in Fig. 14a, the water permeability of the different materials could be easily determined using Equation (1) (see values in Table 2).

Another important issue to consider was that appropriate experimental conditions must be selected to proper compare the bactericidal capacity of the samples. On the one hand, each sample must contain the same amount of bactericidal agent (iodine-coated AC particles). Considering the packing volume fraction of a particle bed (0.54) and the GO of the developed Guefoams (GO = 0.51), it was easy to deduce that Guefoams 1.83 times longer than the particle beds were required (4.29 mm and 7.84 mm were chosen as the height of the particle bed and Guefoams, respectively). On the other hand, the fluid-dynamic conditions in the different samples must be comparable, so a constant fluid velocity of 0.02 ms^{-1} was chosen. Since each material had a specific water permeability, Equation (1) could be used to determine the height of the water column (h in Fig. 4) that exerted the pressure required for water to flow through each material at the specified velocity. The heights ensuring v = 0.02 ms^{-1} in each sample are indicated in Table 2. Antibacterial activity was measured using the percentage inhibition capacity parameter (IC), which is defined as follows:

$$IC = \frac{C_0 - C_f}{C_0} \times 100 \quad (6)$$

where C_o and C_f represent the concentration of E. coli before and after filtration, respectively.

Fig. 15a shows the water permeability results from Table 2 in a bar graph for visual comparison. Table 2 and Fig. 15b demonstrate, for a couple of concentrations of bacteria in water, that the bactericidal activity of the iodine-functionalized samples strongly depended on the structuring of the activated carbon. Interesting enough, non-functionalized (pristine) AC not only lacked antibacterial activity, but also increased the number of live bacteria. This effect was already observed in [40,41]. In the I-AC particle bed, the bactericidal activity reached 7 % and 31 % for 10^2 and 10^1 $CFUml^{-1}$, respectively. The bactericidal capacity of Guefoams was highly dependent on the size of the interconnecting windows, which could alter the fluid dynamic properties of the water as it flowed through the material. Sample G-1, with large windows (about 0.83 mm in average diameter), had an annihilation capacity comparable to that of the packed bed. For Guefoams with windows of about 0.68 mm in average diameter (sample G-2), the annihilation capacity was 9 % and 35 % for the high and low tested bacteria concentrations, respectively. For window sizes of about 0.40 mm in average diameter (sample G-3), the annihilation capacity increased to 12 % (10^2 $CFUml^{-1}$) and 38 % (10^1 $CFUml^{-1}$). As can be seen, the development of a process that allowed the fabrication of Guefoams with tailored windows had the advantage of controlling the permeability and thus the interaction between the bactericidal guest phases and the bacteria-bearing water flowing through the material. Fig. 15b reveals that the bactericidal effect of the I-AC particle bed and G-1 sample was similar, although G-1 had a higher water permeability than the particle bed. This is because the porous structure of Guefoams could create fluid dynamic conditions that optimized the relationship between the fluid-guest phase interaction and the resistance of the material to fluid passage. This enhanced interaction caused by porous cellular structures was previously observed in [26], where the authors placed bactericidal particles with an average diameter of 6 μm in cellular polyvinyl acetate material when conducting bactericidal experiments. To fill a cellular material with particles, they must be small enough to pass through the interconnecting windows between the porous cavities,

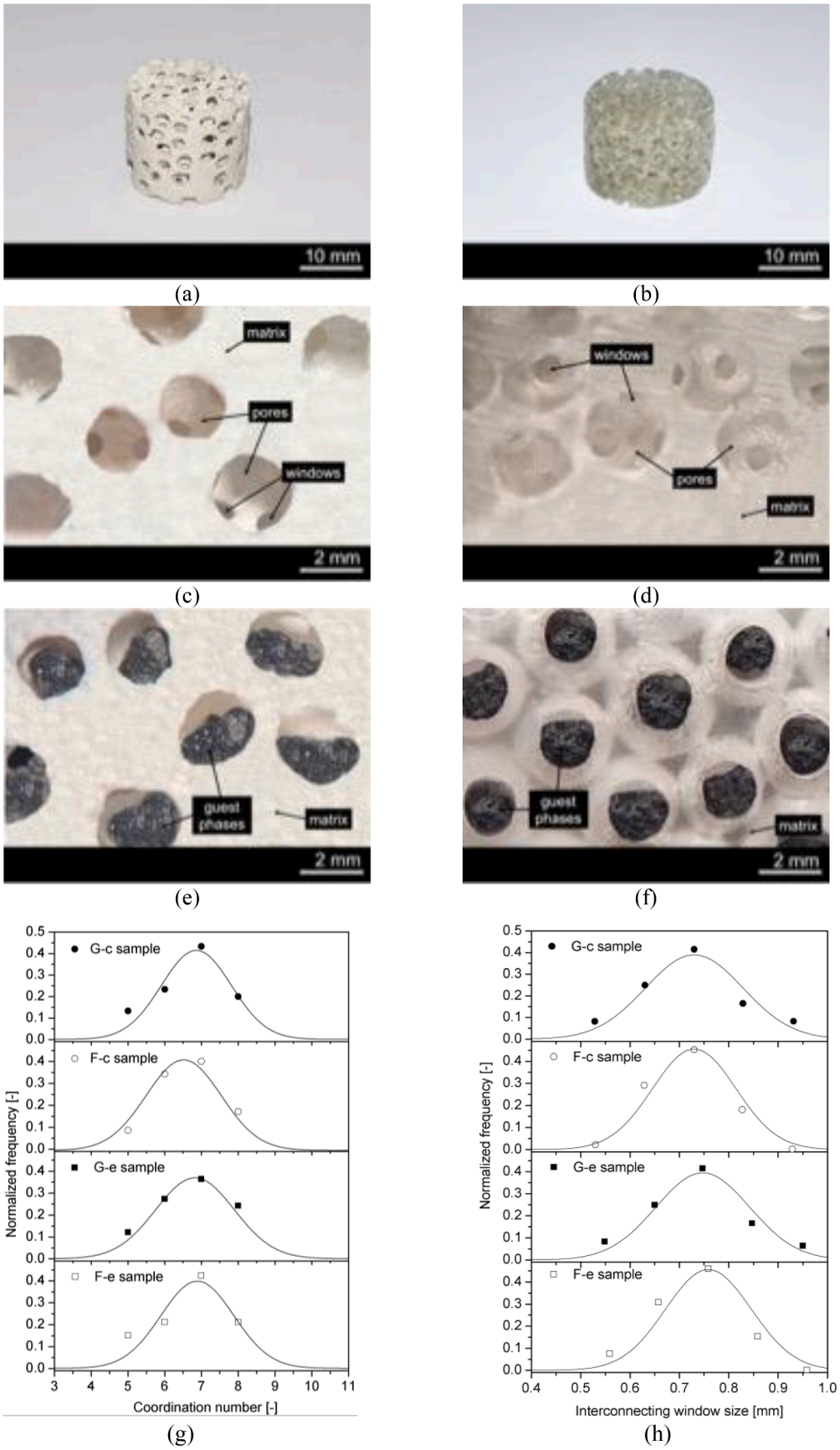

Fig. 12. Photographs of foams prepared using NaCl and paraffin as templating agents by the replication method: cement (a,c) and epoxy (b,d) foams; cement (e) and epoxy (f) Guefoams with AC as the guest phases. In (e,f), the interconnecting windows are concealed beneath the guest phases. (g,h) are distributions of the coordination number and the size of the interconnecting windows for all samples in Table 1.

Table 2
Materials tested in water bacteria removal. The Guefoams contain iodinated activated carbon particles as guest phase, t_s represents the sintering time employed to generate interconnecting windows of diameter d, t_d denotes the time required to remove the double template by ultrasound, k is the water permeability of the tested materials and h is the height of the water in the filtration device. The inhibition capacity (IC) of the materials at two different bacteria concentrations is indicated.

Material	t_s (min)	d (mm)	t_d (min)	k (m^2)	h (cm)	IC (%) (10^1 CFUml^{-1})	IC (%) (10^2 CFUml^{-1})
AC	–	–	–	2.44×10^{-10}	–	<0	<0
I-AC	–	–	–	2.52×10^{-10}	3.33	31	7
G-1	50	0.83	150	1.45×10^{-9}	1.14	28	7
G-2	20	0.68	190	6.80×10^{-10}	2.38	35	9
G-3	10	0.40	240	1.42×10^{-10}	11.57	38	12

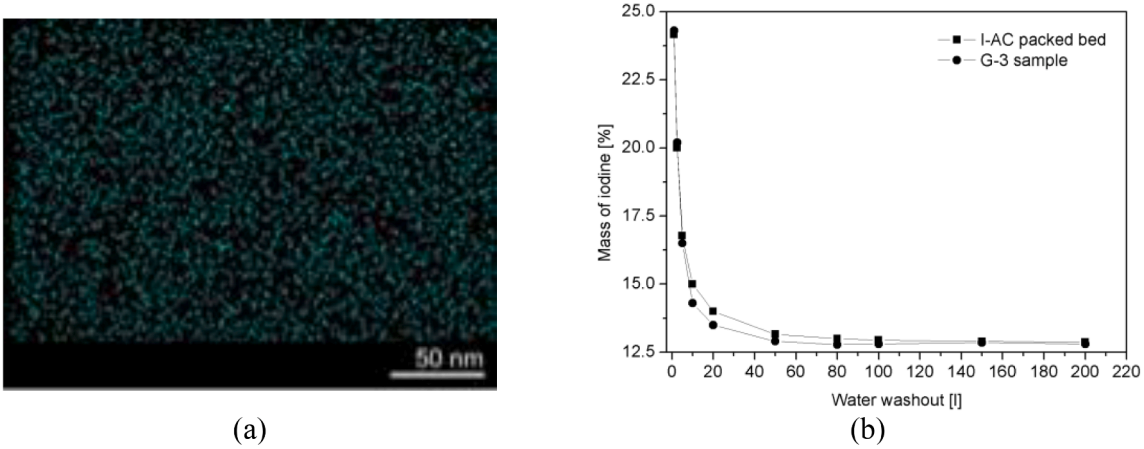

Fig. 13. Elemental mapping microscopy for iodine (a) and quantification of the mass percentage of elemental iodine on the surface of AC particles after injection of selected volumes of water (b).

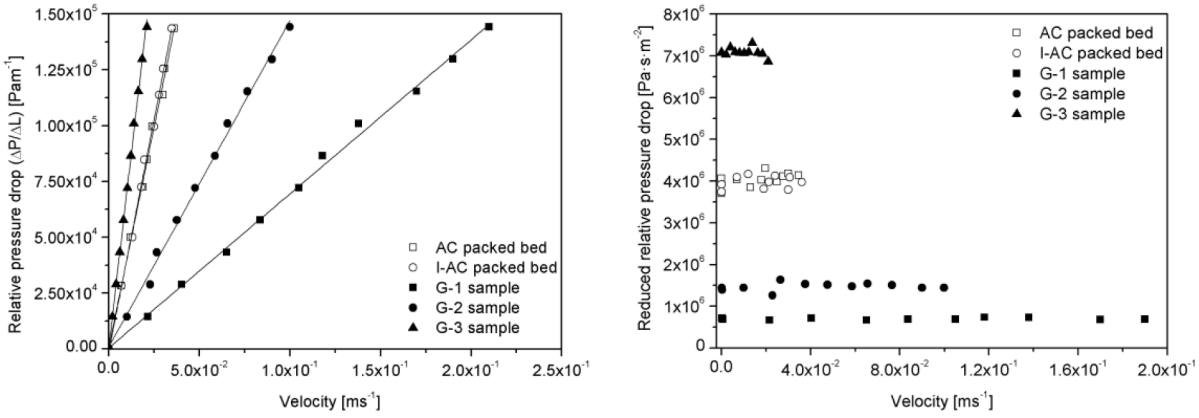

Fig. 14. Relative pressure drop (ΔP/ΔL) (a) and reduced relative pressure drop (ΔP/vΔL) (b) as a function of water superficial velocity for the tested materials. The linear fittings in (a) are: $y = 4.11 \times 10^6 x$ and $R^2 = 0.99$ for AC packed bed, $y = 3.98 \times 10^6 x$ and $R^2 = 0.99$ for I-AC packed bed, $y = 6.93 \times 10^5 x$ and $R^2 = 0.99$ for G-1 sample, $y = 1.48 \times 10^6 x$ and $R^2 = 0.99$ for G-2 sample, and $y = 7.04 \times 10^6 x$ and $R^2 = 0.99$ for G-3 sample.

creating a mixed microstructure involving those of a particle bed and a cellular material. In the case of Guefoams, the guest phase particles (which are not bound to the matrix) have greater mobility than particles in a packed bed. This means that the guest phase particles can move as the fluid flows through them, making their entire surface area available for interaction with the fluid.

In terms of their potential applications, Guefoam materials exhibited equivalent or greater bactericidal activity than a bed of packed particles. However, it is important to consider not only the bactericidal capacity, but also its relationship to economically significant parameters such as the pressure drop required for possible and effective filtration. To comprehensively evaluate the filtration performance of the materials, the compromise parameter of the quality factor (QF) was introduced, which can be calculated as follows [42]:

$$QF = \frac{-\ln\left(\frac{100-IC}{100}\right)}{\Delta P} \quad (7)$$

Fig. 15c depicts the quality factor of the tested materials for bacteria concentrations of 10^1 and 10^2 CFUml^{-1}. Sample G-1 had the highest QF value, as confirmed by the two concentrations tested. This material, despite not having the highest bactericidal activity in absolute terms, had the best ratio of activity per unit of energy consumed (pressure drop) during the passage of water through it, making it an interesting material for industrial applications. It must be emphasized that the primary aim of this study is to highlight the advantages of structuring

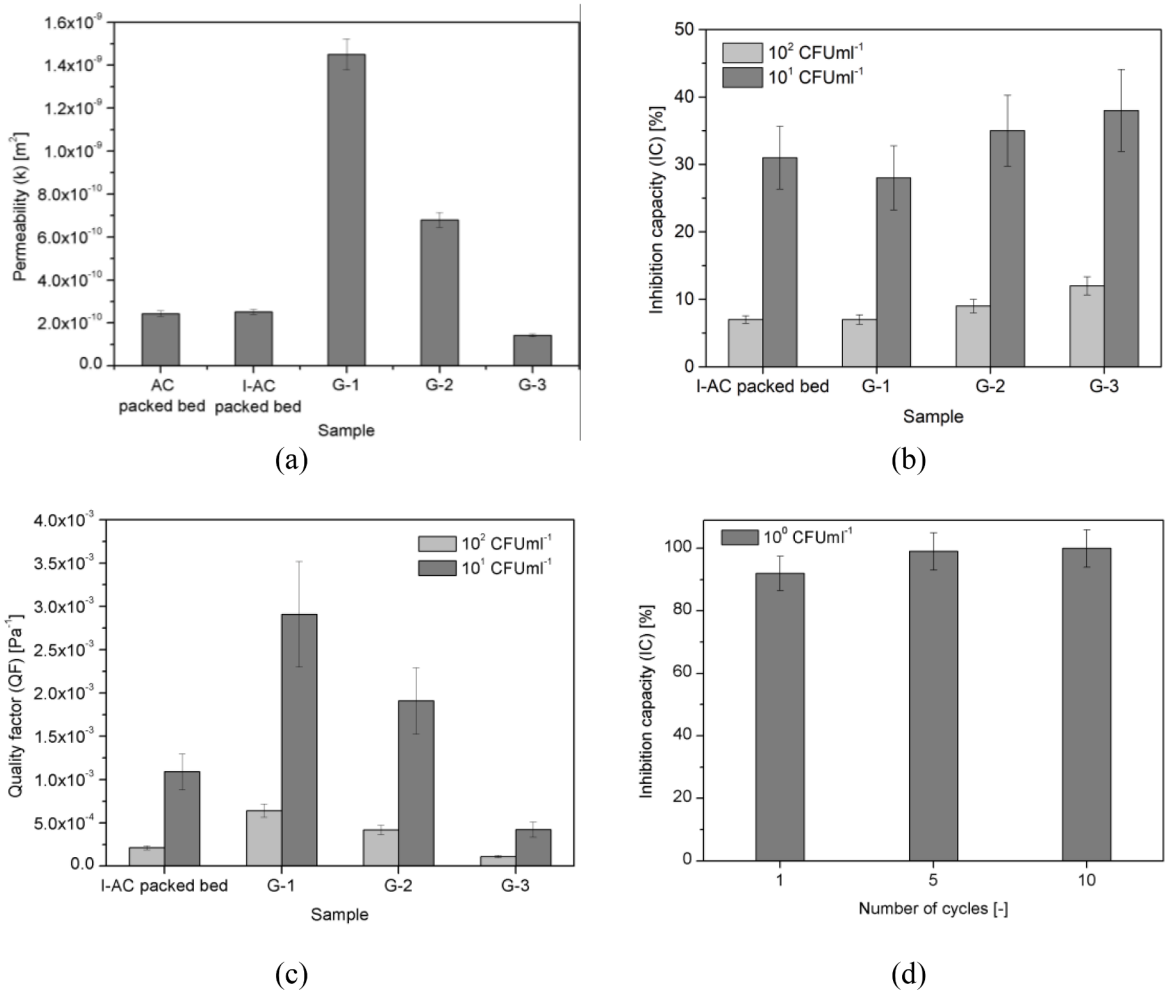

Fig. 15. Water permeability k (a), inhibition capacity IC (b), and quality factor QF (c) for the tested materials. (b) and (c) are given for two concentrations of bacteria. (d) is the inhibition capacity of the G-1 material for different number of consecutive filtration cycles.

bactericidal phases within a Guefoam, as opposed to using conventional particle beds, in the context of filtration efficiency. It is conceivable that extending the length of the bactericidal material bed could augment the chances of achieving effective water purification. Indeed, the literature frequently showcases studies that employ bactericidal particle beds of significant length (roughly ranging from 7 [43] to 100 cm [44]), resulting in reported bactericidal performances close to 100 %. To circumvent the challenge of uniform behavior across the materials tested in this study, thereby rendering meaningful comparisons difficult, columns of material or particle beds were intentionally designed with relatively short lengths (7.8 mm for Guefoams and 4 mm for particle beds). This deliberate choice allowed for a rigorous comparison of bactericidal properties among different mate rials but rendered direct comparisons with existing literature challenging. In addition, a supplementary test was carried out to determine the applicability of the G-1 material in water purification for human consumption, which requires a nil nominal E. coli concentration. For this purpose, 5 l of water containing a bacterial concentration of 10^0 CFUml^{-1} were filtered through the material. The inhibition achieved with a single filtration cycle (one pass through the material of the volume of water considered) was 92 %, but with 5 or 10 cycles, the inhibition was greater than 99 %, demonstrating the high applicability of the developed material (Fig. 15d). In terms of translation to parameters of industrial interest, it could be argued that the effect of n filtration cycles was somehow equivalent to that of n times longer materials. The authors are currently conducting a study focused on investigating the recyclability of the materials developed in this research. Preliminary findings suggest the presence of residual cellular material adhering to the surfaces of the guest phases, resulting from the bacterial lysis process that occurs post-filtration, after their demise. These remnants can be effortlessly removed through brief ultrasound treatment. Moreover, in instances where filtration processes deplete the iodine content to levels that compromise their effectiveness, these materials can be promptly reconditioned to restore their iodine content, thus ensuring their suitability for multiple filtration cycles.

In general terms, the use of Guefoams in bacteria filtration processes offers numerous advantages. Guefoams are monolithic structural materials, which facilitates their handling during material removal and regeneration. In addition, the features shown in Fig. 15a-d demonstrate the superior efficiency of highly permeable Guefoams, which enable significantly less energy-intensive filtration processes.

4. Conclusions

A modification of the replication method involving two combined templating agents (NaCl and paraffin) allowed the preparation of conventional foams and Guefoams with a high degree of microstructural regularity (shape, size and pore size distribution) from both water-based ceramic and polymer precursors. The addition of paraffin as a coating to the NaCl or NaCl-coated particles allowed the formation of binding collars between the particles, which ensured the formation of interconnecting windows in the final material (especially important for highly wetting polymer matrix precursors) and acted as a barrier against

the reaction of NaCl with the infiltration precursor (which is essential when using water-based slurries as precursors for ceramic matrices). The design of the interparticle binding collars, which were converted into interconnecting windows after removal of the template, enabled control of the final material properties. To demonstrate the significance and versatility of the proposed method, foam and Guefoam specimens were fabricated using polymer (epoxy resin) and ceramic (cement) matrices with different window sizes interconnecting their porous architecture. In general terms, the newly developed processing route not only introduced the groundbreaking opportunity to fabricate polymeric or ceramic foam and Guefoam materials using the replication method but also empowered precise control over their fluid-dynamic properties. This control extended to pore shape, size, size distribution, and structural attributes of the guest phases. This development holds profound significance as it paves the way for the straightforward and cost-effective production of non-metallic foam and Guefoam materials. It marks a pivotal milestone in the design and manufacturing of materials tailored with specific characteristics for highly targeted applications.

The authors demonstrated the applicability of a family of materials for water bacteria removal systems. The selected materials were Guefoams consisting of a polymer (epoxy resin) matrix and AC particles with an iodine-functionalized surface. The number and size of the interconnecting windows determined the water permeability and pressure drop in these materials. The materials produced were highly permeable for use in water filtration because they were designed to have interconnecting windows in the range 0.40–0.83 mm. The results showed excellent filtration performance in annihilating E. coli in water, especially for the material with an average window size of 0.83 mm. Its internal pore structure created a strong interaction between the guest phases and the bacteria-bearing water, making it a functionally interesting material with antibacterial activity, comparable to a bed of functionalized AC particles, but with much greater water permeability. Due to the high permeability, the water pressure drop in this material was significantly lower than in a particle bed, making it a highly effective filter. Therefore, the developed materials could be ideal candidates for the future development of energy-efficient and functionally effective filter systems.

Declaration of Competing Interest

The authors declare that they have no known competing financial interests or personal relationships that could have appeared to influence the work reported in this paper.

Data availability

Data will be made available on request.

Acknowledgments

The authors express their gratitude to the Spanish Agencia Estatal de Investigación (AEI), the Spanish Ministry of Science and Innovation, and the European Union for grants PDC2021-121617-C21 and PID2021-127566NB-I00, and the financial support from the Conselleria d'Innovació, Universitats, Ciència, i Societat Digital of the Generalitat Valenciana through grants GVA-COVID19/2021/097 and CIPROM/2021/022.

References

[1] J. Banhart, Manufacture, characterisation and application of cellular metals and metal foams, Prog. Mater Sci. 46 (2001) 559–632, https://doi.org/10.1016/S0079-6425(00)00002-5.
[2] F. García-Moreno, Commercial applications of metal foams: Their properties and production, Materials. 9 (2016) 85, https://doi.org/10.3390/ma9020085.
[3] M. Wang, S. Xu, Preparation and applications of foam ceramics, IOP Conference Series: Earth and Environmental Science. 186 (2018) 012066. Doi: 10.1088/1755-1315/186/2/012066.
[4] L.P. Maiorano, C.Y. Chaparro-Garnica, E. Bailón García, D. Lozano-Castelló, A. Bueno-López, J.M. Molina-Jordá, Guefoams (guest-containing foams) as novel heterogeneous catalysts: Preparation, characterization and proof-of-concept testing for CO2 methanation, Mater. Des. 217 (2022), 110619, https://doi.org/10.1016/j.matdes.2022.110619.
[5] J.M. Molina-Jordá, Highly adsorptive and magneto-inductive Guefoams (Multifunctional Guest-Containing Foams) for enhanced energy-efficient preconcentration and management of VOCs, ACS Appl. Mater. Interfaces 12 (2020) 11702–11712.
[6] J.M. Molina-Jordá, Magneto-inductive open-cell cellular carbon composites with activated carbon as guest phase: Guefoams for energy-efficient VOCs management, Ceram. Int. 48 (2022) 17440–17448, https://doi.org/10.1016/j.ceramint.2022.03.008.
[7] C. Gaillard, J.F. Despois, A. Mortensen, Processing of NaCl powders of controlled size and shape for the microstructural tailoring of aluminium foams, Mater. Sci. Eng. A 374 (2004) 250–262, https://doi.org/10.1016/j.msea.2004.03.015.
[8] R. Goodall, A. Marmottant, L. Salvo, A. Mortensen, Spherical pore replicated microcellular aluminium: Processing and influence on properties, Mater. Sci. Eng. A 465 (2007) 124–135, https://doi.org/10.1016/j.msea.2007.02.002.
[9] A. Jinnapat, A.R. Kennedy, The manufacture of spherical salt beads and their use as dissolvable templates for the production of cellular solids via a powder metallurgy route, J. Alloy. Compd. 499 (2010) 43–47, https://doi.org/10.1016/j.jallcom.2010.03.132.
[10] A. Mortensen, R. Goodall, Method of producing a porous metallic article, European Patent, Ep 2.118.668.B1, (2011) 1–14.
[11] F.Ç. Durmus, L.P. Maiorano, J.M. Molina, Open-cell aluminum foams with bimodal pore size distributions for emerging thermal management applications, Int. J. Heat Mass Transf. 191 (2022), 122852, https://doi.org/10.1016/j.ijheatmasstransfer.2022.122852.
[12] Q. Hou, D.W. Grijpma, J. Feijen, Preparation of interconnected highly porous polymeric structures by a replication and freeze-drying process, J. Biomed. Mater. Res. 67B (2003) 732–740, https://doi.org/10.1002/jbm.b.10066.
[13] C.-J. Liao, C.-F. Chen, J.-H. Chen, S.-F. Chiang, Y.-J. Lin, K.-Y. Chang, Fabrication of porous biodegradable polymer scaffolds using a solvent merging/particulate leaching method, J. Biomed. Mater. Res. 59 (2002) 676–681, https://doi.org/10.1002/jbm.10030.
[14] R.A. White, F.M. Hirose, R.W. Sproat, R.S. Lawrence, R.J. Nelson, Histopathologic observations after short-term implantation of two porous elastomers in dogs, Biomaterials 2 (1981) 171–176.
[15] M. Nofar, J. Utz, N. Geis, V. Altstädt, H. Ruckdäschel, Foam 3D printing of thermoplastics: A symbiosis of additive manufacturing and foaming technology, Adv. Sci. 9 (2022) 2105701, https://doi.org/10.1002/advs.202105701.
[16] F.-L. Jin, M. Zhao, M. Park, S.-J. Park, Recent trends of foaming in polymer processing: A review, Polymers 11 (2019) 953, https://doi.org/10.3390/polym11060953.
[17] G. Wu, P. Xie, H. Yang, K. Dang, Y. Xu, M. Sain, L.-S. Turng, W. Yang, A review of thermoplastic polymer foams for functional applications, J. Mater. Sci. 56 (2021) 11579–11604, https://doi.org/10.1007/s10853-021-06034-6.
[18] Y. Chen, N. Wang, O. Ola, Y. Xia, Y. Zhu, Porous ceramics: Light in weight but heavy in energy and environment technologies, Mater. Sci. Eng. R. Rep. 143 (2021), 100589, https://doi.org/10.1016/j.mser.2020.100589.
[19] A.R. Studart, U.T. Gonzenbach, E. Tervoort, L.J. Gauckler, Processing routes to macroporous ceramics: A Review, J. Am. Ceram. Soc. 89 (2006) 1771–1789, https://doi.org/10.1111/j.1551-2916.2006.01044.x.
[20] C. Vakifahmetoglu, D. Zeydanli, P. Colombo, Porous polymer derived ceramics, Mater. Sci. Eng. R. Rep. 106 (2016) 1–30, https://doi.org/10.1016/j.mser.2016.05.001.
[21] K. Schwartzwalder, A.W. Somers, Method of making porous ceramic articles, U.S. Patent US3090094A. (1963) 4.
[22] H.R. Ramay, M. Zhang, Preparation of porous hydroxyapatite scaffolds by combination of the gel-casting and polymer sponge methods, Biomaterials 24 (2003) 3293–3302, https://doi.org/10.1016/S0142-9612(03)00171-6.
[23] T.J. Fitzgerald, V.J. Michaud, A. Mortensen, Processing of microcellular SiC foams, J. Mater. Sci. 30 (1995) 1037–1045.
[24] R. Prieto, E. Louis, J.M. Molina, Fabrication of mesophase pitch-derived open-pore carbon foams by replication processing, Carbon 50 (2012) 1904–1912, https://doi.org/10.1016/j.carbon.2011.12.041.
[25] R. Goodall, A. Mortensen, Microcellular aluminium? - Child's play!, Adv. Eng. Mater. 9 (2007) 951–954, https://doi.org/10.1002/adem.200700190.
[26] Y. Natori, Y. Kinase, N. Ikemoto, F. Spaziani, T. Kojima, H. Kakuta, J. Fujita, K. Someya, K. Tatenuma, T. Yabuta, H. Takakuwa, K. Otsuki, Activated carbon impregnated with elementary iodine: Applications against virus- and bacteria-related issues, J. Carbon Res. 7 (2021) 86, https://doi.org/10.3390/c7040086.
[27] L.P. Maiorano, J.M. Molina, Challenging thermal management by incorporation of graphite into aluminium foams, Mater. Design. 158 (2018) 160–171, https://doi.org/10.1016/j.matdes.2018.08.026.
[28] S. J. L. Kang, Initial Stage Sintering, Sintering. (2005) 39-55. Doi: 10.1016/b978-075066385-4/50004-2.
[29] G.C. Kuczynski, Study of the Sintering of Glass, J. Appl. Phys. 20 (1949) 1160–1163, https://doi.org/10.1063/1.1698291.
[30] D. Demirskyi, H. Borodianska, D. Agrawal, A. Ragulya, Y. Sakka, O. Vasylkiv, Peculiarities of the neck growth process during initial stage of spark-plasma,

microwave and conventional sintering of WC spheres, J. Alloy. Compd. 523 (2012) 1–10, https://doi.org/10.1016/j.jallcom.2012.01.146.
[31] X. Han, T. Zhao, X. Gao, H. Li, Preparation and characterization of high-temperature non-flowing SiO2/EG/paraffin composites by high-temperature refining, Colloids Surf A Physicochem Eng Asp 542 (2018) 1–7, https://doi.org/10.1016/j.colsurfa.2018.01.043.
[32] P. Manoj Kumar, K. Mylsamy, P.T. Saravanakumar, R. Anandkumar, A. Pranav, Experimental study on thermal properties of nano-TiO2 embedded paraffin (NEP) for thermal energy storage applications, Mater. Today:. Proc. 22 (2020) 2153–2159, https://doi.org/10.1016/j.matpr.2020.03.282.
[33] M. Gönen, D. Balköse, F. İnal, S. Ülkü, The effect of zinc stearate on thermal degradation of paraffin wax, J. Therm. Anal. Calorim. 94 (2008) 737–742, https://doi.org/10.1007/s10973-008-9365-8.
[34] S. Paneliya, S. Khanna, Utsav, A.P. Singh, Y.K. Patel, A. Vanpariya, N.H. Makani, R. Banerjee, I. Mukhopadhyay, Core shell paraffin/silica nanocomposite: A promising phase change material for thermal energy storage, Renewable Energy. 167 (2021) 591–599. Doi: 10.1016/j.renene.2020.11.118.
[35] P. Langston, A.R. Kennedy, Discrete element modelling of the packing of spheres and its application to the structure of porous metals made by infiltration of packed beds of NaCl beads, Powder Technol. 268 (2014) 210–218, https://doi.org/10.1016/j.powtec.2014.08.018.
[36] A. Marmottant, L. Salvo, C.L. Martin, A. Mortensen, Coordination measurements in compacted NaCl irregular powders using X-ray microtomography, J. Eur. Ceram. Soc. 28 (2008) 2441–2449, https://doi.org/10.1016/j.jeurceramsoc.2008.03.041.
[37] A.J. Otaru, H.P. Morvan, A.R. Kennedy, Measurement and simulation of pressure drop across replicated porous aluminium in the Darcy-Forchheimer regime, Acta Mater. 149 (2018) 265–273, https://doi.org/10.1016/j.actamat.2018.02.051.
[38] L. Weber, D. Ingram, S. Guardia, A. Athanasiou-Ioannou, A. Mortensen, Fluid flow through replicated microcellular materials in the Darcy-Forchheimer regime, Acta Mater. 126 (2017) 280–293, https://doi.org/10.1016/j.actamat.2016.12.067.
[39] L.P. Maiorano, R. Castillo, J.M. Molina, Al/Gf composite foams with SiC-engineered interfaces for the next generation of active heat dissipation materials, Compos. Part A: Appl. Sci. Manufactur. 166 (2023), 107367, https://doi.org/10.1016/j.compositesa.2022.107367.
[40] Y. Ge, J. Liu, T. Jiang, Y. Hao, X. Shen, Z. Gong, Z. Qi, J. Yao, Self-disinfecting carbon filter: In situ spontaneous generation of reactive oxidative species via oxygen reduction reaction for efficient water treatment, Colloids Surf A Physicochem Eng Asp 648 (2022), 129266, https://doi.org/10.1016/j.colsurfa.2022.129266.
[41] W.-R. Li, X.-B. Xie, Q.-S. Shi, H.-Y. Zeng, Y.-S. OU-Yang, Y.-B. Chen, Antibacterial activity and mechanism of silver nanoparticles on Escherichia coli, Appl. Microbiol. Biotechnol. 85 (2010) 1115–1122, https://doi.org/10.1007/s00253-009-2159-5.
[42] K.M. Yun, A.B. Suryamas, F. Iskandar, L. Bao, H. Niinuma, K. Okuyama, Morphology optimization of polymer nanofiber for applications in aerosol particle filtration, Sep. Purif. Technol. 75 (2010) 340–345, https://doi.org/10.1016/j.seppur.2010.09.002.
[43] Q.L. Shimabuku, F.S. Arakawa, M. Fernandes Silva, P. Ferri Coldebella, T. Ueda-Nakamura, M.R. Fagundes-Klen, R. Bergamasco, Water treatment with exceptional virus inactivation using activated carbon modified with silver (Ag) and copper oxide (CuO) nanoparticles, Environ. Technol. 38 (2017) 2058–2069, https://doi.org/10.1080/09593330.2016.1245361.
[44] W.A.M. Hijnen, G.M.H. Suylen, J.A. Bahlman, A. Brouwer-Hanzens, G.J. Medema, GAC adsorption filters as barriers for viruses, bacteria and protozoan (oo)cysts in water treatment, Water Res. 44 (2010) 1224–1234, https://doi.org/10.1016/j.watres.2009.10.011.